Journal of the Meteorological Society of Japan, Vol. 88, No. 3, pp. 475–496, 2010.
DOI:10.2151/jmsj.2010-313

Formation of Tropical Cyclones in the Northern Indian Ocean Associated with Two Types of Tropical Intraseasonal Oscillation Modes

Kazuyoshi KIKUCHI and Bin WANG

International Pacific Research Center, University of Hawaii, Honolulu, Hawaii, USA

(Manuscript received 1 June 2009, in final form 18 November 2009)

Abstract

Over the northern Indian Ocean (NIO), a substantial number (~ 60%) of tropical cyclones (TCs) form in association with significant intraseasonal oscillation (ISO) events (i.e., Nargis [2008]). In this paper the relationship between TC genesis and ISO in the NIO was studied using 30-year (1997–2008) observations. Because NIO TCs mainly occur in transitional seasons when climatological environmental forcing favors TC genesis, two types of ISO modes, boreal summer intraseasonal oscillation (BSISO) and Madden-Julian oscillation (MJO), which represents boreal winter ISO, were objectively and quantitatively defined, and their connection with TC genesis was examined. It was found that over 70% of ISO-related genesis is associated with the northward propagating BSISO mode and up to 30% with the eastward propagating MJO mode. The BSISO mode primarily affects TC formation in May–June and September–November, while the MJO mode affects TC formation primarily from November–December. Because of their distinct structures and lifecycles, the BSISO and MJO modes affect TC formation differently. For the BSISO mode, TC formation is enhanced during its wet phases overlaying the NIO. For the MJO mode, TC formation is enhanced after the convection passes over the Malay Peninsula and when the Indian Ocean is in a dry phase. The BSISO mode enhances TC genesis by creating favorable environmental forcing for TC genesis, while the MJO mode does not. The most salient feature is that both the ISO modes favor TC genesis by providing a synoptic-scale seeding disturbance at least six days prior to TC formation. The seeding disturbance provided by the BSISO is a cyclonic vorticity anomaly to the north of the equatorial convection/westerly wind burst, whereas the seeding provided by the MJO is a convectively coupled Rossby wave that breaks away from the major body of the MJO convection. The seasonality of the NIO TC genesis, intensity, and prevailing tracks are also explained in terms of the effect of environmental forcing on TC genesis potential, steering flow, and maximum potential intensity. The results imply that monitoring the evolution of the two types of ISO modes, especially the BSISO, may provide a useful medium-range forecast for NIO cyclogenesis.

1. Introduction

Tropical cyclones (TCs) (also referred to as hurricanes, typhoons, or storms depending on the ocean basin) are characterized by strong winds and torrential rain. They are a major focus in tropical meteorology because of their serious, and sometimes devastating, effect on human activities. The energetic nature of TCs is often viewed as a Carnot engine (Emanuel 1986); warm waters with a sea surface temperature (SST) greater than 26°C was recognized as a necessary condition for TC formation several decades ago (Palm'en 1948). Six parameters consisting of three dynamic conditions (low-level relative vorticity, the Coriolis parameter, and tropospheric vertical wind shear) and three thermodynamic conditions (SST, conditional instability, and midtropospheric relative humidity) were suggested as crucial parameters for TC formation (Gray 1968, 1979). Thus far, six basins, including western and eastern North Pacific, North Atlantic, north Indian Ocean, south Indian Ocean, and

Corresponding author: Kazuyoshi Kikuchi, International Pacific Research Center, University of Hawaii, 1680 East West Road, POST Bldg. 401, Honolulu, HI 96822, USA.
E-mail: kazuyosh@hawaii.edu

South Pacific, have long been recognized as major TC formation regions (Riehl 1948). In these regions, with the exception of the northern Indian Ocean (NIO), summer is the period in which the six necessary conditions that favor TC formation occur. In spite of the early realization of the existence of the six major basins for TC formation, most efforts have focused on the North Pacific and Atlantic, due partly to the large number of TC occurrence there and partly for economic reasons.

While the number of TCs occurring in the NIO is relatively small, a strong TC in this region could be extremely deadly because of its proximity to dense population areas. The TC Nargis that emerged in the Bay of Bengal in April 2008, and battered Myanmar was one of them. Storm surge on top of strong winds and torrential rainfall reportedly caused over 130,000 fatalities. This tragic event underscores the need for scientists to advance our knowledge and improve forecasting of TCs in the NIO. A number of articles that examine different aspects of Nargis have already been published in major journals (Shi and Wang 2008; Webster 2008; Kikuchi et al. 2009; Lin et al. 2009; Reale et al. 2009), and this special issue by the Journal of the Meteorological Society of Japan is intended to focus on lessons learned from Nargis.

Numerous fundamental questions regarding TCs in the NIO have yet to be answered. Among those issues, TC formation or cyclogenesis is one of the most significant and least understood processes. In general, it is widely believed that a TC does not arise spontaneously even if the necessary conditions are satisfied (Riehl 1948; Bergeron 1954; Rotunno and Emanuel 1987). In addition to the aforementioned necessary conditions, a finite amplitude disturbance characteristic of waves with 1,000–3,000-km wavelength (Emanuel 2003) that acts as a seed is usually required for cyclogenesis. As a result, cyclogenesis may be viewed as a stochastic process subject to environmental forcing determined by a set of necessary conditions and weather noise primarily determined by short-term tropical disturbances (Emanuel and Nolan 2004).

The likelihood of TC genesis is thus affected by multiple-scale variations from day-to-day weather to interdecadal change. On a subseasonal time scale, a substantial part of tropical disturbances are closely related to various types of convectively coupled equatorial waves (CCEWs) (Takayabu 1994; Wheeler and Kiladis 1999; Kiladis et al. 2009). Thus, the CCEWs appear to affect the likelihood of TC genesis. Note that the definition of CCEWs in the present study is somewhat broadened for convenience; thus, easterly waves and Madden-Julian oscillation (MJO) (Madden and Julian 1971, 1972) are both included.

Easterly waves have long been known to initiate TCs in the Atlantic (Landsea et al. 1998; Thorncroft and Hodges 2001), eastern North Pacific (Avila 1991; Molinari et al. 1997), and western North Pacific (Briegel and Frank 1997; Ritchie and Holland 1999). Dickinson and Molinari (2002) showed that mixed Rossby-gravity waves may become TCs through a transformation to a tropical-depression-type disturbances (Takayabu and Nitta 1993; Zhou and Wang 2007). Some other processes are also considered to affect the likelihood of TC formation by modifying environmental forcing, such as increasing low-level cyclonic circulation or weakening the vertical shear of horizontal winds to facilitate the development of an incipient disturbance. Recently, a number of studies focused on this aspect and suggested that the equatorial Rossby wave and MJO with a characteristic 30–60-day period have a large influence on cyclogenesis and rapid intensification in many basins (Maloney and Hartmann 2000a, b; Molinari and Vollaro 2000; Bessafi and Wheeler 2006; Frank and Roundy 2006; Zhou and Wang 2007), with heavy emphasis on the western and eastern North Pacific.

Despite recent advancements, our knowledge about how CCEWs affect cyclogenesis in the NIO is still very limited. The NIO is controlled by a very energetic Asian monsoon system. Therefore, in contrast to other basins, TC occurrence in the NIO has two distinctive peaks in the pre- and post-monsoon seasons because the strong vertical shear during the summer monsoon season suppresses TC development. This complex situation makes TC formation events relatively rare, unique, and complicated and consequently, our progress in understanding NIO TC dynamics has been slow.

In order to fill this gap, we carried out a pilot study to elucidate how Nargis formed in association with the MJO (terminology will be carefully defined in this paper to avoid confusion) using multiple satellite observations (Kikuchi et al. 2009). In that study, we proposed a new scenario that a synoptic scale disturbance associated with the Tropical intraseasonal oscillation (ISO) becomes a TC. The purpose of this study is to test, consolidate, and generalize this novel scenario by conducting a statistical analysis based on a 30-year dataset. Note

that the ISO over the NIO contains two components, the 30–60 day and the quasibiweekly wave (QBW). On the basis of spectrum analysis, we can reasonably separate these disturbances (Kikuchi and Wang 2009). While the QBW plays an important role in modifying the activity of synoptic-scale disturbances during boreal summer (Goswami et al. 2003), our analysis first focuses on the 30–60-day component of the ISO to simplify the discussion. Special attention is paid to comparing the Nargis case and general statistical analysis in hopes that the result will be useful for other case studies (Kunii et al. 2010; Yamada et al. 2010; Yokoi and Takayabu 2010) or modeling studies (Kuroda et al. 2010; Saito et al. 2010; Taniguchi et al. 2010; Yanase et al. 2010; Yoshida et al. 2010) targeting Nargis. One of the new contributions of this study lies in the careful treatment of the ISO. The two ISO modes are separated, and their connections to cyclogenesis are examined.

Section 2 documents the data and methodology in which the genesis potential index (GPI) that measures the environmental forcing and the classification of the ISOs are explained. In section 3, we examine some aspects of TC behaviors and their association with environmental forcing in the NIO. The relationship between cyclogenesis and two ISO modes are examined in section 4. A possible physical underlying mechanism that connects cyclogenesis and ISO is discussed in section 5 and a summary of our findings is presented in section 6.

2. Data and methodology

2.1 Data

We used several datasets provided by different platforms for the period 1979–2008 to ensure the quality and availability of the marine data. For TC formation, the best track data compiled by Joint Typhoon Warning Center (JTWC) were used, which provide information about locations, time, and strength (maximum sustained surface wind speed) of disturbances in 6 h intervals. Genesis time was defined as when a disturbance was first classified as a tropical depression in the NIO with maximum sustained surface wind speed exceeding 17 knots, which is in line with previous studies (Molinari and Vollaro 2000; Frank and Roundy 2006). Daily outgoing longwave radiation (OLR) data with a horizontal resolution of $2.5^\circ \times 2.5^\circ$ in longitude and latitude (Liebmann and Smith 1996) were used to depict organized convection and as a good proxy for precipitation falling from deep convection in the tropics. Daily National Centers for Environmental Prediction–Department of Energy (NCEP–DOE) Atmospheric Model Intercomparison Project (AMIP)-II reanalysis data with a horizontal resolution of $2.5^\circ \times 2.5^\circ$ (Kanamitsu et al. 2002) were used to describe large-scale circulation. Reynold's SSTs (Reynolds et al. 2002) were used to calculate environmental forcing (Emanuel 2000). The original resolution was $1^\circ \times 1^\circ$ but was reduced to $2.5^\circ \times 2.5^\circ$ for our study.

The Japan Meteorological Agency (JMA) 25-year Reanalysis (JRA-25) (Onogi et al. 2007) and JMA/Climate Data Assimilation System (JCDAS) were used to examine the relationship between cyclogenesis and synoptic-scale disturbances associated with the ISO. These data are homogeneous datasets with JRA-25 covering the period 1979–2004, and JCDAS taking over from 2005. They are good at representing TCs in terms of location and strength using wind profile retrieval technique (Hatsushika et al. 2006). Horizontal winds at 850 hPa with 6 hour temporal resolution and T106 horizontal resolution (equivalent to about 1.125° resolution), one of the highest resolution data they provide, were used in this study. To extract a synoptic-scale disturbance, a technique based on spatial filtering developed by Kurihara et al. (1993) was used, in which a three-point moving average is applied in longitudinal and latitudinal directions multiple times. Kurihara (1993) applied the moving average to data with a horizontal resolution of $1^\circ \times 1^\circ$, while we applied it to the original data ($\sim$1.125°). We checked that this treatment makes little difference.

2.2 Genesis potential index (GPI)

As discussed in section 1, TC genesis may be viewed as a stochastic process subject to the environmental forcing and weather noise. To measure the effect of environmental forcing on cyclogenesis the GPI, which was developed by Emanuel and Nolan (2004), was computed. This index is similar to the one first proposed by Gray (1979). The major difference is that Emanuel and Nolan (2004) incorporated the effect of SST continuously by using maximum potential intensity (MPI) instead of threshold SST.

The GPI is expressed as

$$GPI = |10^5\eta|^{3/2}\left(\frac{\mathscr{H}}{50}\right)^3\left(\frac{V_{pot}}{70}\right)^3(1+0.1V_{shear})^{-2}, \quad (1)$$

where η is the absolute vorticity at 850 hPa (s^{-1}),

$\mathscr{H}$ is the relative humidity in the middle troposphere (%), V_{pot} is the MPI in terms of wind speed (ms^{-1}), and V_{shear} is the magnitude of the vertical wind shear between 850 hPa and 200 hPa (ms^{-1}). The MPI, which is based on an axisymmetric steady-state model of a mature TC, gives an upper bound on TC intensity that can be written as

$$|V_{pot}|^2 = \frac{T_s}{T_0}\frac{C_k}{C_D}(CAPE^* - CAPE), \qquad (2)$$

where T_s is the ocean surface temperature, T_0 is the mean outflow temperature, C_k is the exchange coefficient for enthalpy, C_D is the drag coefficient, $CAPE^*$ is the convective available potential energy of air lifted from saturation at sea level in reference to the environmental sounding at the radius of maximum winds, and $CAPE$ the convective available potential energy of boundary layer air (Bister and Emanuel 2002). After some manipulation, it was shown that the SST, pressure, vertical profiles of temperature, and specific humidity are necessary to calculate the MPI at each grid point. The definition of middle troposphere for the use of $\mathscr{H}$ is somewhat different among literatures, e.g., 600 hPa in Nolan et al. (2006) and Camargo et al. (2007a) and 700 hPa in Emanuel and Nolan (2004) and Camargo et al. (2007b). Here we use the 600-hPa but the choice of either level makes little difference. GPI provides an expected number of storms per decade per 2.5° square of latitude and longitude under a given environmental forcing (Nolan et al. 2006).

Calculation of both GPI and MPI was carried out similar to the way as Emanuel (2000) calculated MPI. Namely, daily MPI was computed using NCEP-DOE daily reanalysis data and linearly interpolated Reynolds SST data. Monthly data were then obtained by averaging the daily data for each month in each year. Similarly, monthly GPI data was computed using NCEP-DOE daily data by averaging the daily GPI data. Note that monthly GPI obtained by averaging daily GPI and directly from monthly data are qualitatively consistent.

Fig. 1, for example, shows climatological TC occurrence and GPI in the NIO as a function of month. GPI captures well the seasonal cycle in TC occurrence; the twin peaks in pre- and post-monsoon seasons and reductions in February–March and July–August. A more detailed examination of GPI will be given in section 3.1.

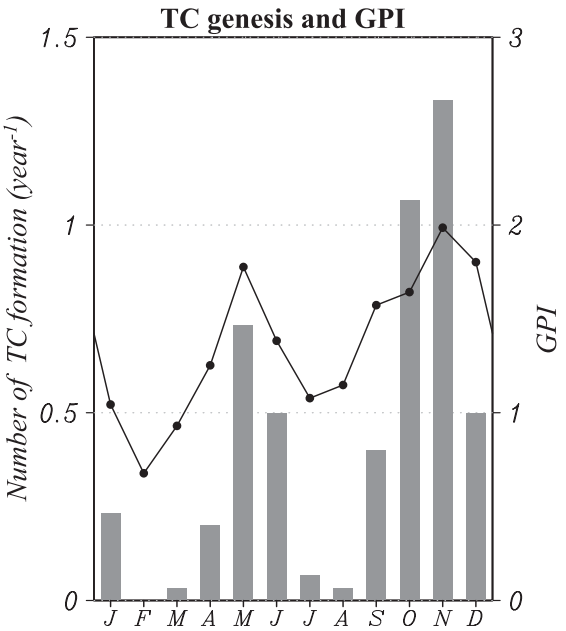

Fig. 1. Climatological likelihood of TC genesis (bar) and expected likelihood from environmental conditions in terms of TC genesis potential index (GPI) (solid line) averaged in the NIO (0°–30°N, 40°–100°E) for 1982–2008 as a function of calendar month. The time at which TC formation took place is based on the time when storms reached tropical-depression strength.

2.3 Two ISO modes: BSISO and MJO

The properties of the ISO are strongly affected by the annual cycle in the background conditions such as SST, and consequently, large-scale atmospheric circulations as demonstrated by Wang and Xie (1997). The ISO activity is strongest in the boreal winter and weakest in the boreal summer (Gutzler and Madden 1989; Salby and Hendon 1994; Zhang and Dong 2004). A meridional shift in major ISO activity is also observed (Salby and Hendon 1994; Kemball-Cook and Wang 2001). The latitudinal band of strong ISO activity shifts to the south of the equator in boreal winter and to the north of the equator in boreal summer, in line with the meridional shift of the tropical convergence zone.

The meridional shift in ISO activity appears to be related to two different propagation behaviors of the ISO (Lau and Chan 1985, 1986; Wang and Rui 1990). During the boreal summer convection associated with the ISO tends to show a northward movement in the NIO (Yasunari 1979; Sikka and Gadgil 1980) as well as a weak eastward movement along the equator. During the boreal winter, how-

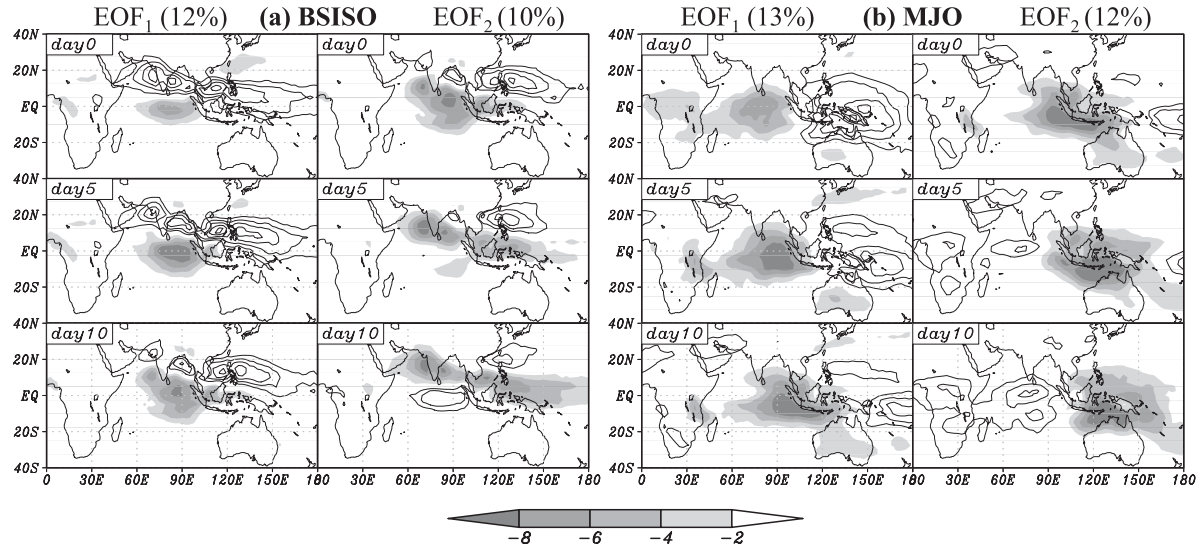

Fig. 2. Spatiotemporal patterns of the extended EOF (EEOF) modes obtained for boreal (a) summer (JJA) and (b) winter (DJF) for the period 1979–2008. The left (right) panel shows the first (second) mode. The EEOF analysis with three different time steps with 5-day increments was performed by using 30–60-day filtered OLR data. OLR values are normalized by multiplying one standard deviation of the corresponding principal component. Negative (positive) values are shaded (contoured), and the contour interval is 2 Wm^{-2}. The zero contour is suppressed.

ever, an eastward propagation of convection along the equator is predominant in the western hemisphere (Lau and Chan 1985; Weickmann et al. 1985) and can be seen even in the eastern hemisphere as a circumnavigation signal (Kikuchi and Takayabu 2003). Of course there are other minor variations in behaviors of the ISO, particularly during transitional seasons such as spring and fall, which were not considered in this study on the basis of a sensitivity test carried out (not shown) and the results of a previous study (Kemball-Cook and Wang 2001). Because the two ISO modes have different associated circulation structures (Hendon and Salby 1994; Maloney and Hartmann 1998; Kemball-Cook and Wang 2001), it is expected that their roles in TC genesis are different; a careful examination of the relationship between TC genesis and two types of ISO is required. Given that TC occurrence in the NIO has two peaks in spring and fall (Fig. 1), during which the selection of the preferred intraseasonal mode strongly depends on the year, the idea of treating the summer and winter modes separately can be justified. From now on, we refer to boreal summer ISO as BSISO, as in Fu and Wang (2004), and boreal winter ISO as MJO.

a. Identification of BSISO and MJO events

A simple, consistent method was used to identify BSISO and MJO modes. First, a Lanczos bandpass filter (Duchon 1979) with a cut-off periods of 30 and 60 days is applied to daily OLR data to extract the variations associated with the ISO. Then, an extended empirical orthogonal function (EEOF) analysis (Weare and Nasstrom 1982) with three time steps and five-day increments is applied to the filtered OLR data in the tropical-subtropical eastern hemisphere (40°S–40°N, 0°–180°). The only difference between identifying the BSISO and MJO modes is the data period to which the EEOF analysis was applied. For the BSISO mode, the filtered OLR data from June through August is used and for MJO mode the data from December through February is used.

As shown in a similar analysis by Lau and Chang (1985; 1986), the EEOF analysis gives concise and fair representations of both modes by combining the first two EEOFs (Fig. 2). It is clear that just putting the first two EEOFs represents a half cycle of each mode. The BSISO mode (Fig. 2a) captures the northward movement in the NIO, which eventually makes an elongated convective band tilting from northwest to southeast and covers a

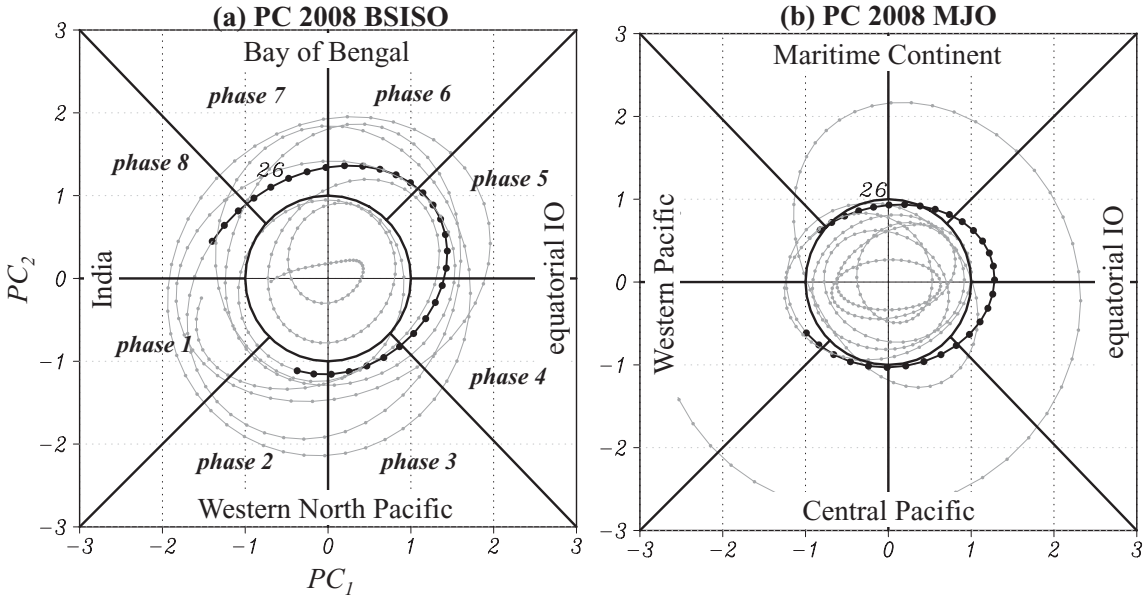

Fig. 3. An example of phase-space representation of the (a) BSISO and (b) MJO for 2008. The abscissa and ordinate are the normalized PC_1 and PC_2 (by one standard deviation of each component), respectively, during (a) JJA and (b) DJF. The trajectory in April 2008 is indicated by the thick line with dots. The four locations shown in each panel indicate where most organized convection associated with each mode is present in a given phase.

wide range from the Arabian Sea to the western Pacific. This feature is in good agreement with a recent composite study using TRMM satellite data (Wang et al. 2006). The MJO mode (Fig. 2b) shows a predominantly eastward propagation along the equator that is in accordance with the classical view of the MJO (Madden and Julian 1972).

b. Composite method

Because the first two EEOFs are predominant and their combination represents a half life cycle of the BSISO or MJO mode, it is natural to consider a phase-space representation spanning the first two leading principal components (PCs), as in previous studies (e.g., Kikuchi and Takayabu 2003; Wheeler and Hendon 2004). The detailed procedure is as follows. 1) An entire time series for the PCs of the first two EEOFs for both the BSISO and MJO modes are obtained by projecting the two EEOFs on filtered OLR data so that we can describe the state of each mode at any particular time. 2) The PCs are normalized by one standard deviation of the corresponding PCs to gauge the strength of the ISO at a given time. Note that one standard deviation is computed for the corresponding period in the EEOF calculation instead of the entire time series, namely JJA for the BSISO mode and DJF for the MJO mode. 3) The phase-space representation composed of the first two normalized PCs for the BSISO and MJO modes is obtained. Significant ISO events were picked up when its normalized amplitude (square root of the normalized PC_1 plus PC_2) is greater than unity.

Figure 3 shows an example of the phase-space representation for the BSISO and MJO modes in 2008. In this study, the phase is separated into eight categories, as in Wheeler and Hendon (2004). With reference to Nargis, the time series during April is indicated by thick dots and curves. The ISO event that generated Nargis in April, including the time when Nargis emerged as a tropical depression at 18 UTC 26 April, was clearly a predominant BSISO mode (Fig. 3a). This was expected from our previous study (Kikuchi et al. 2009), where we observed the northward movement of convection and a slantwise rainband. Note that we previously referred to this event as the MJO because we did not distinguish between the BSISO and the MJO in that paper. Note also that the MJO signal of the April 2008 event was not really strong especially around the time when Nargis was formed (26 April). Because both modes share some common

characteristics such as eastward propagation in the Indian Ocean (Fig. 2), the amplitude of both modes were relatively strong during the period when the convection associated with the ISO moved eastward along the equator in the Indian Ocean (mid-April) (Figs. 3a, 3b). However, the MJO signal became weaker after the northward propagation of the convection in the NIO became predominant. Figure 3 also shows that the BSISO mode appears to be dominant almost the entire year of 2008. This may be an interesting topic for a future study on interannual variations of the ISO.

c. Identification of predominant mode

Both modes share some common characteristics at specific phases, and accordingly, sometimes both the modes become significant at the same time; therefore, we need to identify which mode is more predominant at a given time to avoid double counting. Because the predominant mode is thought to have a larger variance, we can start by comparing the following reconstructed field represented by the first two EEOFs:

$$\mathbf{OLR}_{BSISO}(t) = \mathbf{EEOF}_{1,BSISO} \times PC_{1,BSISO}(t) + \mathbf{EEOF}_{2,BSISO} \times PC_{2,BSISO}(t), \quad (3)$$

$$\mathbf{OLR}_{MJO}(t) = \mathbf{EEOF}_{1,MJO} \times PC_{1,MJO}(t) + \mathbf{EEOF}_{2,MJO} \times PC_{2,MJO}(t), \quad (4)$$

where $\mathbf{OLR}(t)$ is the reconstructed spatiotemporal pattern, including 5- and 10-day predictions at time t. Subscripts BSISO and MJO indicate each mode; note that *PCs* are not the normalized. Given that $\|EEOF_m\| = 1$ (m is any integer) and the inner product between different eigenvectors becomes 0, (3) and (4) become

$$\|\mathbf{OLR}_{BSISO}(t)\| = \sqrt{PC^2_{1,BSISO}(t) + PC^2_{2,BSISO}(t)} \quad (5)$$

$$\|\mathbf{OLR}_{MJO}(t)\| = \sqrt{PC^2_{1,MJO}(t) + PC^2_{2,MJO}(t)}. \quad (6)$$

It turns out that it is quite simple to evaluate which mode is predominant. This means that we can judge whether any given date during the entire period should be assigned to active BSISO, active MJO, or inactive ISO.

On the basis of the discussion above, a composite life cycle of the BSISO and MJO mode was constructed using 30–60-day filtered OLR data and 850-hPa horizontal winds from NCEP-DOE AMIP-II reanalysis. We will discuss this further in section 4 of this paper. The information about TC formation was also collected if either BSISO or MJO mode was active when a TC formed.

3. Overview of climatological TC formation and intensity in the northern Indian Ocean

Because behaviors of TCs in the NIO have not been well documented, this section focuses on depicting the climatological tendency of TC genesis and intensity in this region in association with the environmental forcing.

3.1 TC formation and GPI

As shown in Fig. 1, the climatological GPI represents climatological annual cycle in TC formation in the NIO overall well. In this section we examine the relationship in more detail (Fig. 4) and also describe the tendency of TC motion. Spatial distribution of the GPI and TC formation is roughly well correlated. Namely, TC formation is likely to occur over a region with a large GPI, which is especially clear in October and November. However, sometimes there is a discrepancy between the location of a GPI maximum and TC formation, which is shown to occur in January, April, and May. One possible reason of this is that this figure does not reflect the interannual variations of the GPI.

Notwithstanding the minor discrepancy just mentioned above, the GPI is expected to be a meaningful predictor of TC formation when taking an average over a wide region (e.g., Fig. 1). If that is the case, it gives us a better chance to think about the reason why TC formation is enhanced or hindered in a given season. Because the GPI is expressed by a nonlinear combination of four parameters [eq. (1)], a careful examination such as changing only one parameter with the other parameters fixed is necessary to examine its breakdown. Such a careful examination indicates the following reasoning to drive the annual cycle in GPI in the NIO. First, the reason why GPI is kept low in boreal summer is the strong vertical wind shear associated with monsoon circulation and a relatively low MPI. On the other hand, the middle-level relative humidity and low-level vorticity provide a preferable condition for TC formation. As a result of the combination of these factors, a weak preferable condition appears along the boundary of the Indian subcontinent and Indochina Peninsula. TCs rarely formed, but monsoon lows and depressions are frequently formed in this region during boreal summer (Gos-

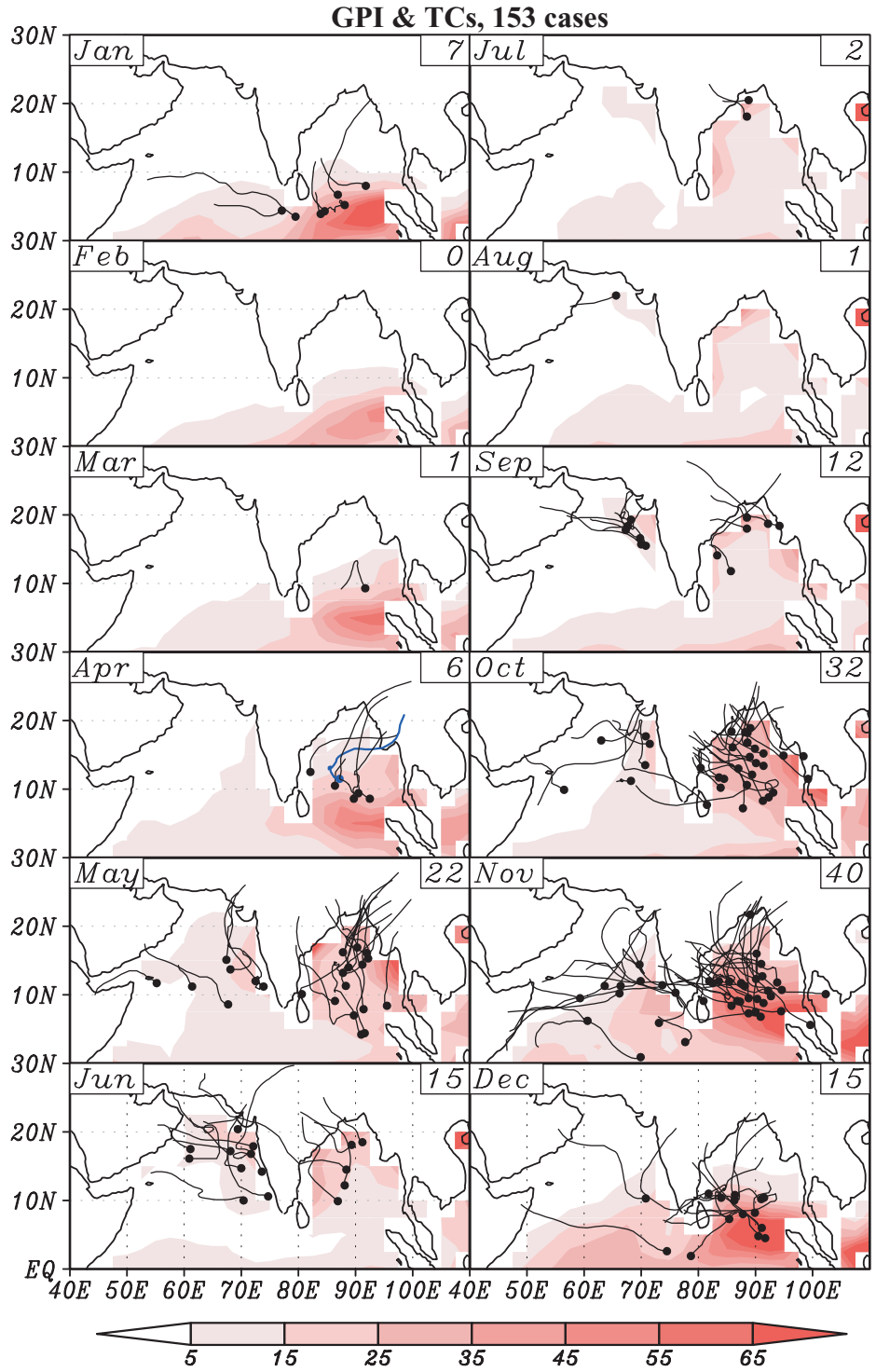

Fig. 4. Climatological monthly-mean genesis potential index (GPI) (shading) derived for the period 1982–2008 together with TC formation events (solid dots) and their tracks (curves) for the period 1979–2008. Formation location and time are decided when a disturbance is first classified as a tropical depression according to JTWC. Each number in the upper right corner of each panel is the total number of formation events that occurred in the corresponding calendar month. Nargis is denoted by the blue dot and curve.

wami et al. 2003) due to the shear instability associated with the monsoon trough energized by moist convection (Goswami et al. 1980; Mak 1987; Shukla 1987). On the other hand, the opposite situation happens in pre- and post-monsoon seasons. Middle-level relative humidity and low-level vorticity do not necessarily provide enough preferable conditions. However, the reduced vertical wind shear and high MPI are responsible for keeping the GPI relatively high in those seasons. A further discussion of the annual cycle of the MPI shall be made later.

Another aspect we would like to address here is the annual variation of TC track. The TC track shows strong seasonality. In April and May, many TCs show northeastward or even eastward propagation in the northern Bay of Bengal, and consequently, hit the west coast of the Indochina Peninsula. Nargis was one of them. In October and November, which are the most active months for TC formation, on the other hand, most of the TCs tend to move northwestward or northward, and consequently, rarely hit the west coast of the Indochina Peninsula. A further discussion of TC motion in the NIO especially focusing on Nargis is given by Yamada et al. (2010) in this special issue. They suggest that the eastward movement of Nargis was attributed to a subtropical jet, which was located along the southern rim of the Tibetan Plateau. In reality, most part of TC motion could be understood in terms of steering flow (George and Gray 1976; Brand et al. 1981); however, several interaction processes such as the interactions between TC vortex and the planetary vorticity gradient (beta drift) (Adem 1956; Holland 1983; Wang and Li 1992) and between TC vortex and convective heating (Wang and Holland 1996; Dengler and Reeder 1997) create a deviation from the path expected from the steering flow. Thus, a further examination is necessary to add the accuracy of our understanding of TC motion in the NIO.

3.2 TC intensity and MPI

We have just seen the annual variation of TC occurrence and motion tendency. Naturally, the next issue of interest will be the annual variation of TC intensity. Namely, was Nargis an exceptionally strong TC or a normal strength TC that occurred in April? As shown in equation (1), GPI includes MPI in its definition. While GPI has been empirically developed, in essence, researchers developed MPI from a theoretical viewpoint (Miller 1958; Emanuel 1997; Holland 1997). The idea of MPI is to provide an upper intensity bound that a TC can achieve under certain atmospheric and oceanic conditions. In reality, almost all TCs cannot achieve MPI strength due primarily to the destructive processes that are not included in the formulation of MPI, such as the existence of the vertical shear of the horizontal wind, feedback from ocean cooling, and the internal variability associated with phenomena such as concentric eyewall cycles (Emanuel 2000). TC-intensity forecasting has lagged far behind the forecasting of TC track (Camp and Montgomery 2001). However, one important implication made by Emanuel (2000) from a statistical viewpoint on the basis of the data over the North Atlantic and western North Pacific basins, is that a given storm is equally likely to attain any intensity between TC force and its MPI.

This implication appears to hold true even in the NIO (Fig. 5). The likelihood of becoming a strong TC is well predicted from the annual cycle in MPI. Similar to GPI, the MPI also has twin peaks in its annual cycle. While the most salient feature is that the likelihood has a pronounced peak in the pre-monsoon season, especially April, instead of the post-monsoon season. Of the six storms that occurred during that period, four of them achieved supercyclonic storm strength. Nargis was not one of them, but it was only a little weaker than that criterion. Nargis is considered to be a typical TC for April in terms of strength.

Why do TCs that occur in April, instead of during the post-monsoon season, tend to be strongest? In other words, why does a TC formed under what should be non-optimal conditions have a better chance of becoming a strong TC than one formed easily under more favorable conditions? On the basis of the above discussion, we believe that analyzing MPI may provide a way to answer this question. As shown in equation (2), the MPI is determined by the difference between $CAPE^*$ and CAPE. Thus, the difference comes from the difference of temperature and humidity between the ocean surface and the air near surface. A careful examination suggests that it is mainly the humidity difference that is responsible for making the annual cycle in MPI in the NIO (figure not shown), and that the annual cycle is closely related to the Asian monsoon (AM) (Goswami 2005; Wang et al. 2005). One of the notable features of the AM annual cycle is its asymmetricity: abrupt onset and gradual retreat. In the pre-monsoon season (April and May),

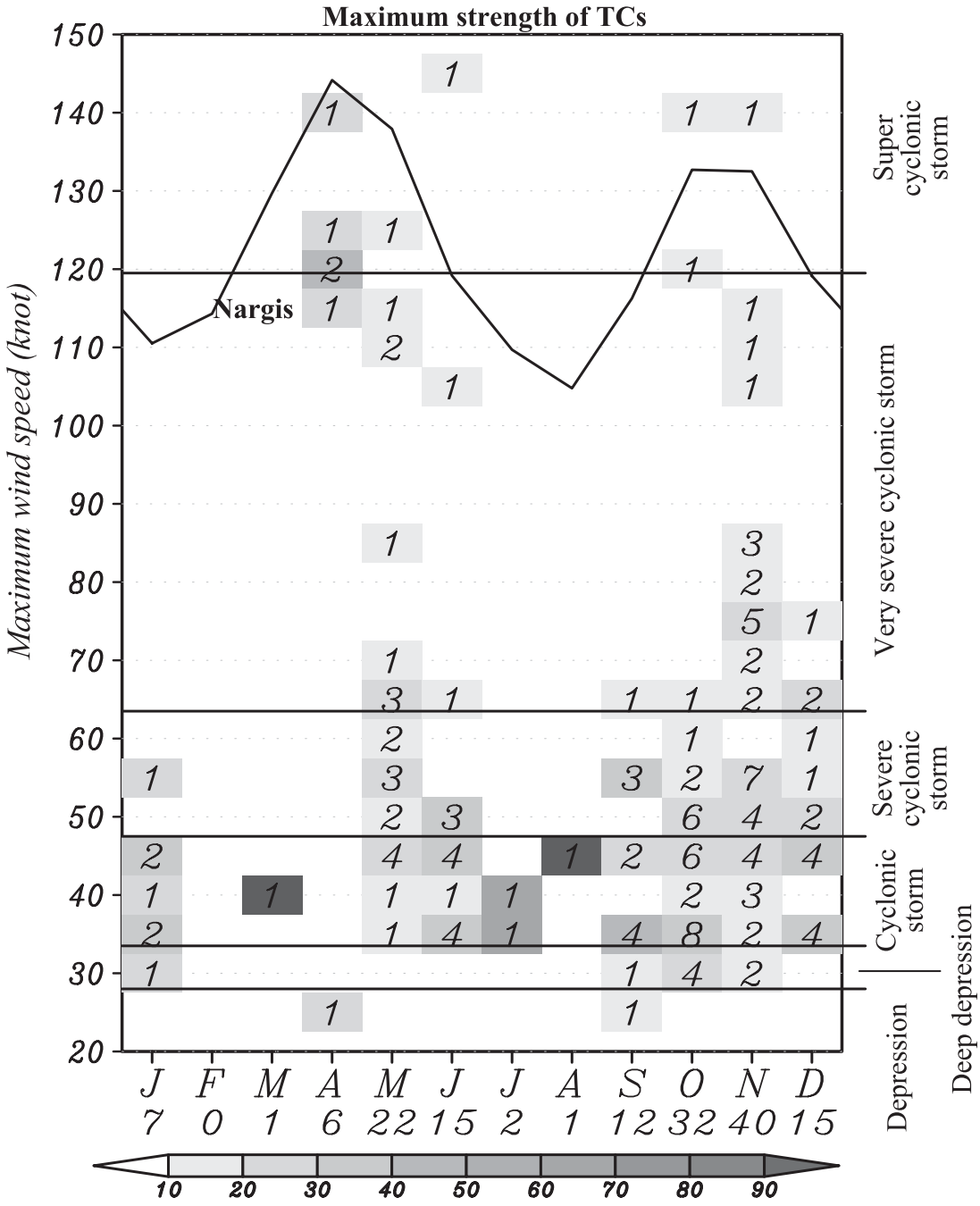

Fig. 5. Cumulative number of TCs occurring in different calendar months (abscissa) as binned by its maximum wind (ordinate) during 1979–2008. The shading represents percentile in each month. The climatological maximum potential intensity derived from 1982–2008 averaged in the northern Indian Ocean (NIO) (0°–30°N, 40°–100°E) is also shown by the solid curve in the top portion of the figure. Terminology for TCs used in the NIO is shown at the right.

convection is mainly seen in the Maritime Continent and is virtually absent in the NIO. Relative humidity is kept low due to the subsidence caused by convection over the Maritime Continent, although SST is kept high during this period (~28°C) (Locarnini et al. 2006). In contrast, the

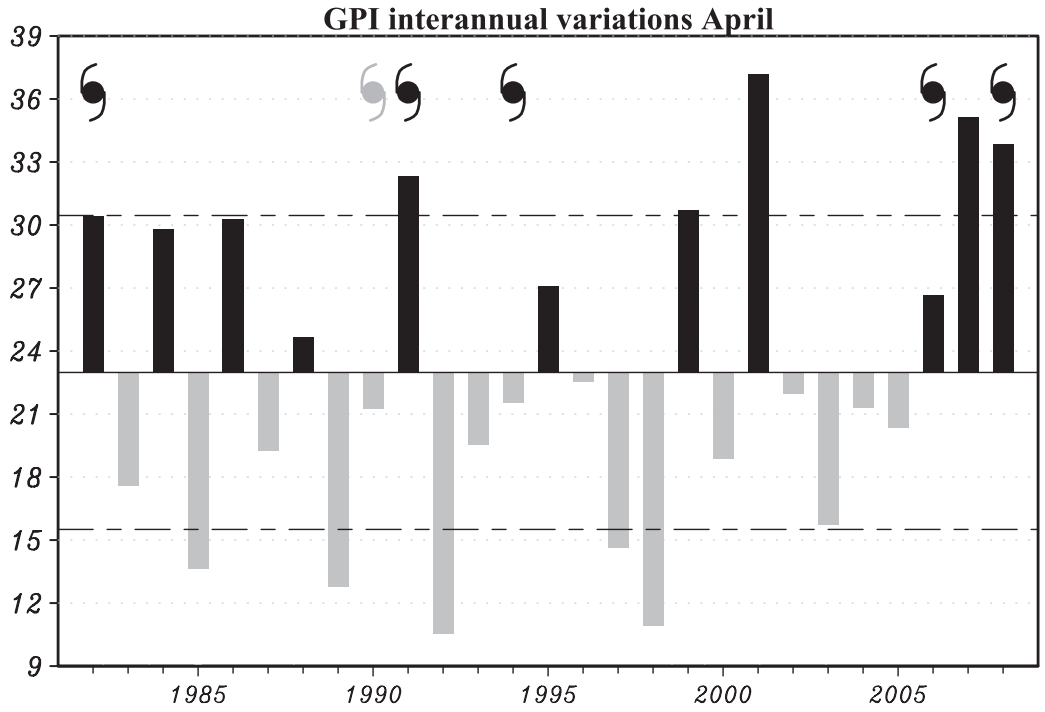

Fig. 6. Interannual variation of genesis potential index (GPI) (bars) together with the occurrence of strong (weak) storms designated by dark (light) weather symbols in April. GPI is an average value over the Bay of Bengal (0°–30°N, 77.5°–100°E). Dash-dotted lines represent one standard deviation of the GPI in April.

gradual retreat of the AM keeps moderate to high relative humidity in the post-monsoon season (October and November) in the NIO, although SST in the post-monsoon season is lower than in the pre-monsoon season by about 1–2°C. Therefore, the MPI in the NIO tends to be high in the pre-monsoon season in which a saturated parcel coming from the ocean surface can obtain more CAPE than that in the boundary layer with a lower humidity content.

3.3 GPI and Nargis: Interannual variability

As discussed above, TCs that occur in the pre-monsoon season, specifically April, have a better chance of becoming the most deadly storms. The ability to forecast the likelihood of TC formation is a critical skill to lessen the damage by these TCs. Given that GPI is able to accurately follow the climatological annual cycle in TC-formation likelihood (Fig. 1), it is natural to wonder if GPI is also able to predict the likelihood of TC formation on an interannual time scale. In particular, we examine the relationship for the month of April (Fig. 6).

Historically, there were five strong storms and one weak storm that occurred during this month (Fig. 5). Finding a good relationship between TC formation and GPI is not necessarily easy because of the stochastic nature of the TC-formation process and unique geolocational situation of the NIO, which is surrounded by Indian subcontinent, Arabian Peninsula, and Indochina Peninsula. Three strong storms emerged under large GPI conditions (1982, 1991, and 2008), two other storms emerged under relatively small GPI conditions (1990 and 1994), and one storm emerged under just the above-normal GPI condition (2006). The difficulty in finding a good relationship between GPI and TC formation is in good agreement with the recent analysis done by Camargo et al. (2007a). They reported that the NIO is the only basin in which no significant relation between the number of TCs and GPI on interannual time scale is found in any season on the basis of a 35-year correlation analysis. If we assume that the TC-formation process in the NIO is still viewed as the same stochastic process as in the other basins, we may be able to make the following conclusions. Unlike other basins, the NIO has fewer weather noises that can act as seeds for TCs, such as easterly waves, primarily

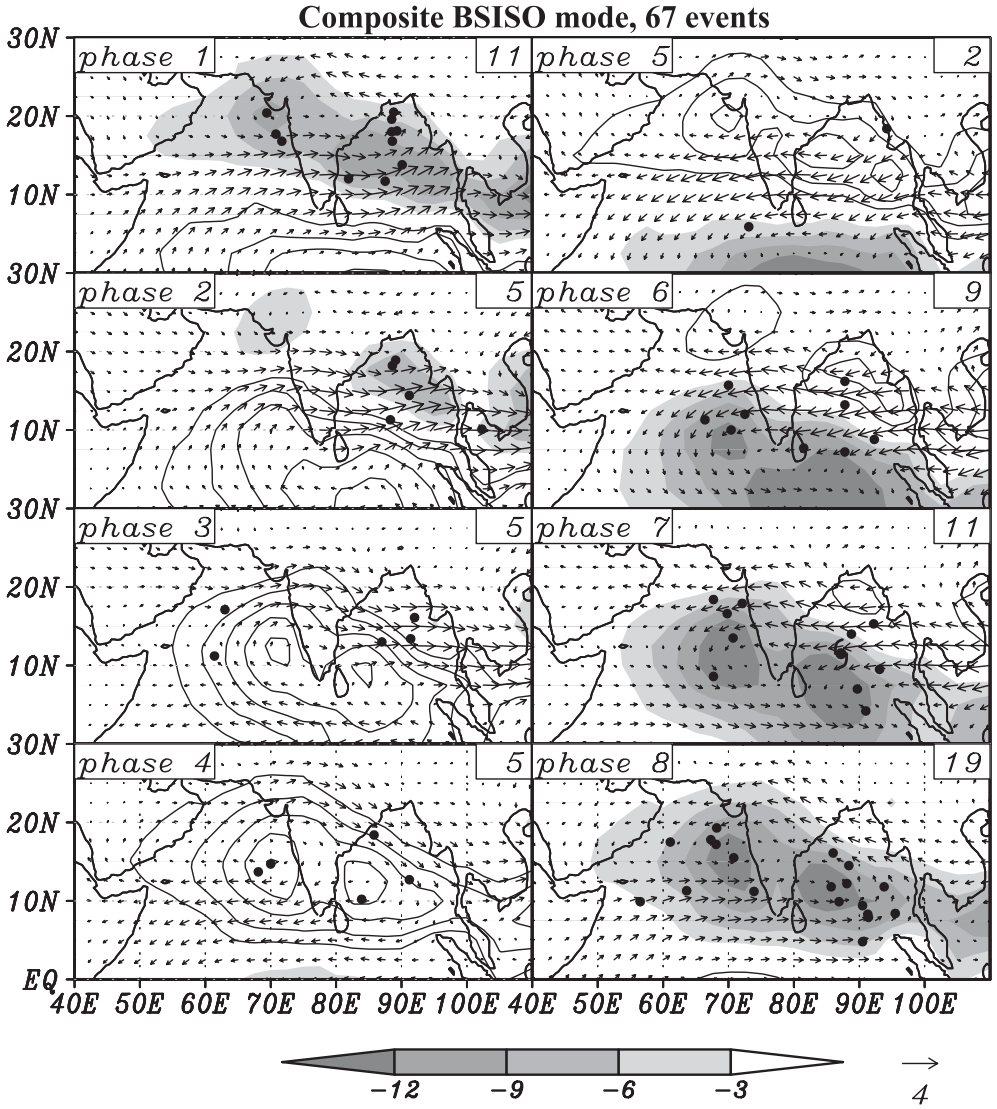

Fig. 7. Composite OLR (shading), 850-hPa horizontal winds (vectors), and TC formation (dots) for events associated with the BSISO mode. The numbers in the upper right corner of each panel represent the total number of TC formation events that occurred in the corresponding phase. Nargis is shown by the TC symbol in phase 7.

due to the unique geolocational situation. Therefore, a larger GPI does not necessarily lead to a higher likelihood of TC formation because of insufficient weather noise. At any rate, an important thing to note here is that GPI in April 2008, during which Nargis formed, was significantly large.

4. TC formation associated with two types of ISO modes

Having discussed some aspects of TC behavior and their association with environmental forcing in the previous section, in this section we investigate the relationship between TC formation and the two ISO modes, BSISO and MJO. We present the composite results in 4.1 and 4.2, and an integrated view in 4.3.

4.1 The BSISO mode

It is beyond doubt that the composite BSISO lifecycle shown in Fig. 7 exactly follows the BSISO lifecycle represented by the two EEOFs (Fig. 2a). A large-scale cyclonic (anticyclonic) circulation in

the lower troposphere accompanies enhanced (suppressed) convection, moving northward. As a result, the NIO undergoes two phases—wet and dry.

Figure 7 indicates that two distinctive phases affect the likelihood of TC formation. TC formation is enhanced during the wet phase (phases 1 and 6 through 8) when it overlays the NIO. The wet phase accounts for most TC formation, which is nearly 75% of the total number of 67 classified as being associated with significant BSISO events. Given that most TC formation events seem to take place between 5°N and 15°N in the Bay of Bengal and 10°–20°N in the Arabian Sea associated with the BSISO mode, it is no wonder that most TC formation events occur in phase 8 where enhanced convection as well as the associated low-level cyclonic circulation is present.

Nargis is typical of the TCs that occur in the wet phase of the BSISO mode. Yet, the underlying physical and dynamical processes of how the BSISO mode affects the likelihood of TC formation in general are not obvious. The previous analysis of Nargis formation by Kikuchi et al. (2009) is helpful in understanding these processes. According to their conclusion, Nargis was transformed from a synoptic-scale disturbance characteristic of a low-level cyclonic circulation coupled with deep convection associated with a BSISO event. The nature of the northward movement of the BSISO mode would facilitate further development of the disturbance. A further discussion will be presented in section 5.2.

4.2 MJO mode

Like the BSISO, the composite MJO life cycle (Fig. 8) exactly follows the MJO life cycle shown by the two EEOFs (Fig. 2b). Namely, the MJO convection is characterized by an eastward propagation along the equator with a small southward shift (Fig. 2b). There are, thus, no apparent wet and dry phases that largely affect precipitation in the NIO, as they do in the BSISO mode. For convenience we refer to the phases 4 to 7 as ''wet'' and the other phases as ''dry''. Without a northward propagation of convection in the NIO, a less-apparent large-scale cyclonic circulation in the lower troposphere is found in the wet phase.

Consequently, the impact of the MJO mode on TC formation appears to be much less compared to the BSISO case; only 25 genesis cases were associated with significant MJO events in contrast to 67 cases associated with significant BSISO events. TC formation is only slightly enhanced by the wet phase of the MJO mode over the Indian Ocean. The most significant impact occurs during phase 8, which is one of the dry phases, of the MJO mode when the active convective area passes through Malay Peninsula. A more detailed analysis of the different impacts of the BSISO and MJO mode will be discussed in section 5.2.

4.3 An integrated view

We found that the number of TC formation events associated with the BSISO mode is about three times higher than those associated with the MJO mode. To understand the relative role of the BSISO and MJO modes in TC formation in terms of the annual cycle, we show the number of TC formation events related to a particular phase of significant BSISO or MJO events together with the climatological amplitude of each mode as a function of the calendar month in Fig. 9. As expected, the amplitude of the BSISO mode is largest during boreal summer and that of the MJO mode, during boreal winter. Yet, the MJO mode has larger seasonality. Climatologically, the seasonal transition of the ISO occurs in April and October when one mode becomes more predominant and the other becomes less predominant in terms of their amplitudes.

TC formation related to each mode reflects the annual cycle. Most TC formation events during boreal summer from May to October are associated with the BSISO mode and those during boreal winter from December to March are associated with the MJO mode. Interestingly, November, instead of October, is considered to be a ''break-even'' season as well as April when the two modes have comparable influences on TC formation. This feature probably reflects the fact that the preference for the mode in those months is most susceptible to the interannual variations of the ISO.

Our strategy of treating the ISO events on the basis of the two ISO modes appears to work well. TC events are equally picked up in any month proportional to the likelihood of TC occurrence (Fig. 1). In addition, TC events that are associated with a certain phase of the BSISO or MJO mode are evenly distributed in each month that is proportional to the likelihood of TC occurrence. We can, therefore, conclude that a TC event can be treated reasonably well throughout the year, no matter when it occurs.

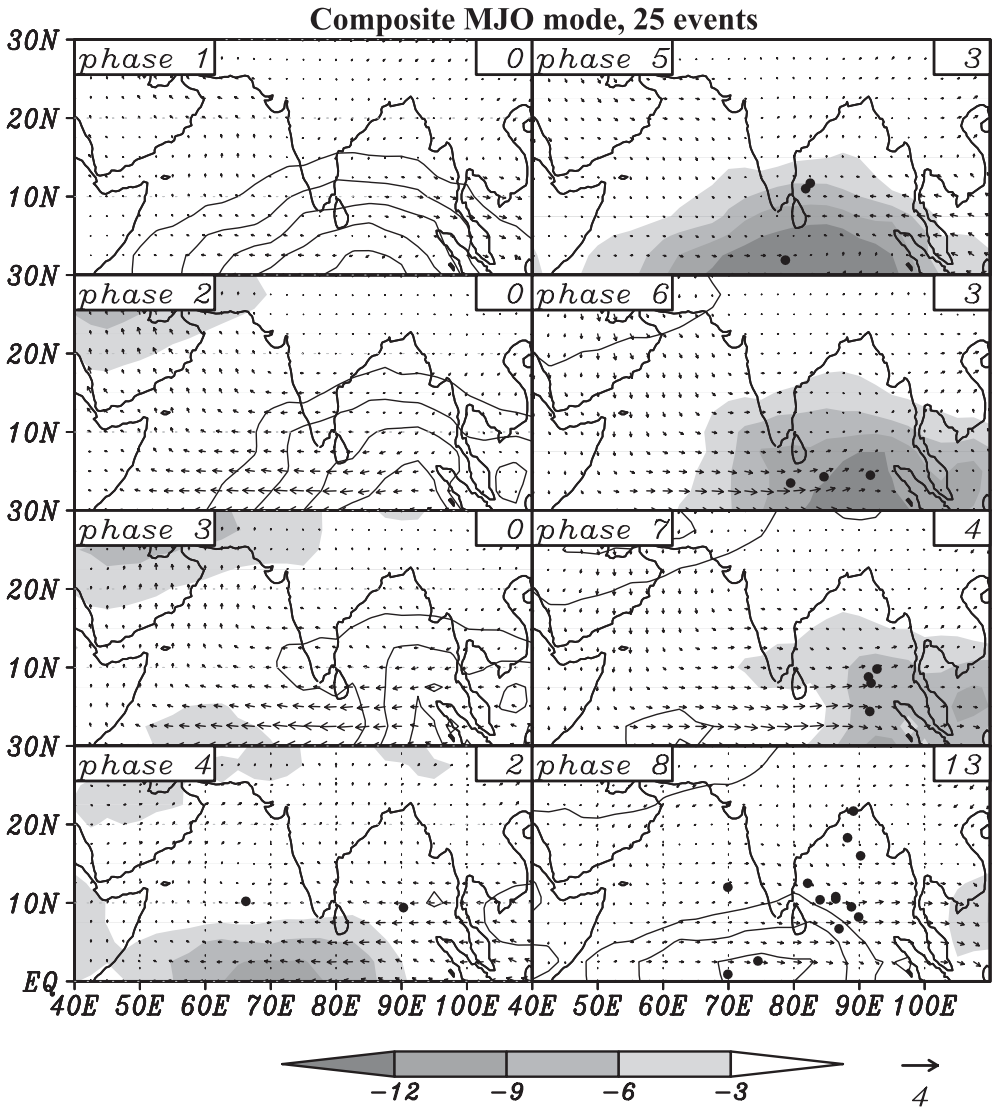

Fig. 8. Same as in Fig. 7, except for the events associated with the MJO mode.

5. What is the role of the ISO in NIO TC genesis?

As shown in the previous section, a substantial part of TC formation is related to a certain phase of the ISO. But how does ISO contribute to TC formation? Because TC genesis is viewed as a stochastic process and ISO is a multi-scale system, the ISO may affect TC formation in two different ways: by modifying the large-scale environmental forcing and by providing a seed disturbance. Because of its multiscale nature, separating the two roles perfectly is difficult, however, the analyses shown here were carried out in an attempt to elucidate the potential role of the ISO in the two aspects discussed above.

5.1 Does ISO change the likelihood of TCs by modifying GPI?

The first question we would like to raise is whether the ISO modulates the likelihood of TC occurrence by changing the environmental forcing. Since the ISO is often characterized by planetary-scale circulation, it is usually thought to act as a modifier of the environmental conditions such as low-level vorticity, vertical shear of the horizontal wind, midtropospheric relative humidity, and MPI [eq. (1)] on an intraseasonal time scale. For instance, any wet phase of the BSISO mode has a low-level large-scale cyclonic circulation (Fig. 7). A

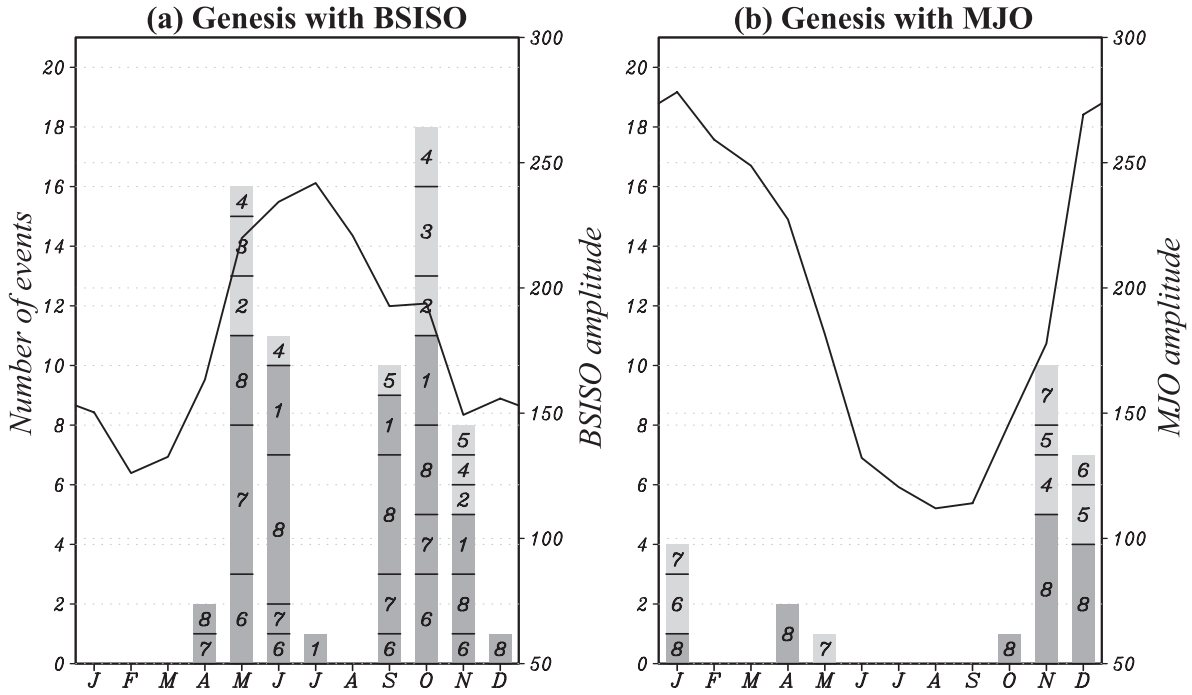

Fig. 9. Number of TC formation events (ordinate) that occurred in association with the (a) BSISO mode and (b) MJO mode during each calendar month for the period 1982–2008. Each number inside a bar bin represents the phase of each ISO mode. Phases that have high likelihood in the composite (Figs. 7 and 8) are shown by darker colors. The solid curves indicate the annual variation of the amplitudes of the (a) BSISO and (b) MJO modes represented by equations (5) and (6), respectively.

passage of the wet phase of the BSISO mode is, therefore, expected to modify the environmental condition and make it more conducive for TC formation, at least from the view point of low-level circulation.

Figure 10 shows the horizontal distribution of composite GPI for TC formation with reference to the inactive and active phases of the BSISO and MJO modes. Because the actual variation of the GPI is caused by the annual cycle plus the ISO, the two major seasons for TC formation associated with the BSISO mode were treated separately. Consequently the two seasons, pre- and post-monsoon, for the BSISO mode and November-to-January season for the MJO mode are presented here. For the BSISO mode, GPI becomes two–three times higher in phase 8 (active phase for TC formation) than in phase 4 (inactive phase for TC formation) in the pre- and post-monsoon seasons (Figs. 10a–10d). The higher GPI correlates with the active convective region of the BSISO mode (Fig. 7) and TC formation.

On the other hand, for the MJO mode the relationship is quite different. The GPI becomes twice as high in phase 4 (inactive phase for TC formation) than in phase 8 (active phase for TC formation). The higher GPI occurs to the east of the active convection region of the MJO mode (Fig. 8). In phase 8, most TC formation events take place in the Bay of Bengal around 10°N. A clue to understanding why higher GPI associated with the MJO mode does not lead to a higher probability of TC formation events will be discussed in the next subsection.

5.2 *Could ISO provide a seed for TC genesis?*

As discussed in section 1, the ISO is thought to encompass some synoptic scale disturbances. Therefore, the second question we would like to address is whether the ISO can act to increase weather noise or provide more seed disturbances for TC formation. In order to answer this question, we conducted a detailed analysis of composite cases using JRA's high-resolution reanalysis data (Fig. 11). As explained in section 2.1, the synoptic-scale horizontal wind component was extracted by Kurihara's method. A composite was then constructed with

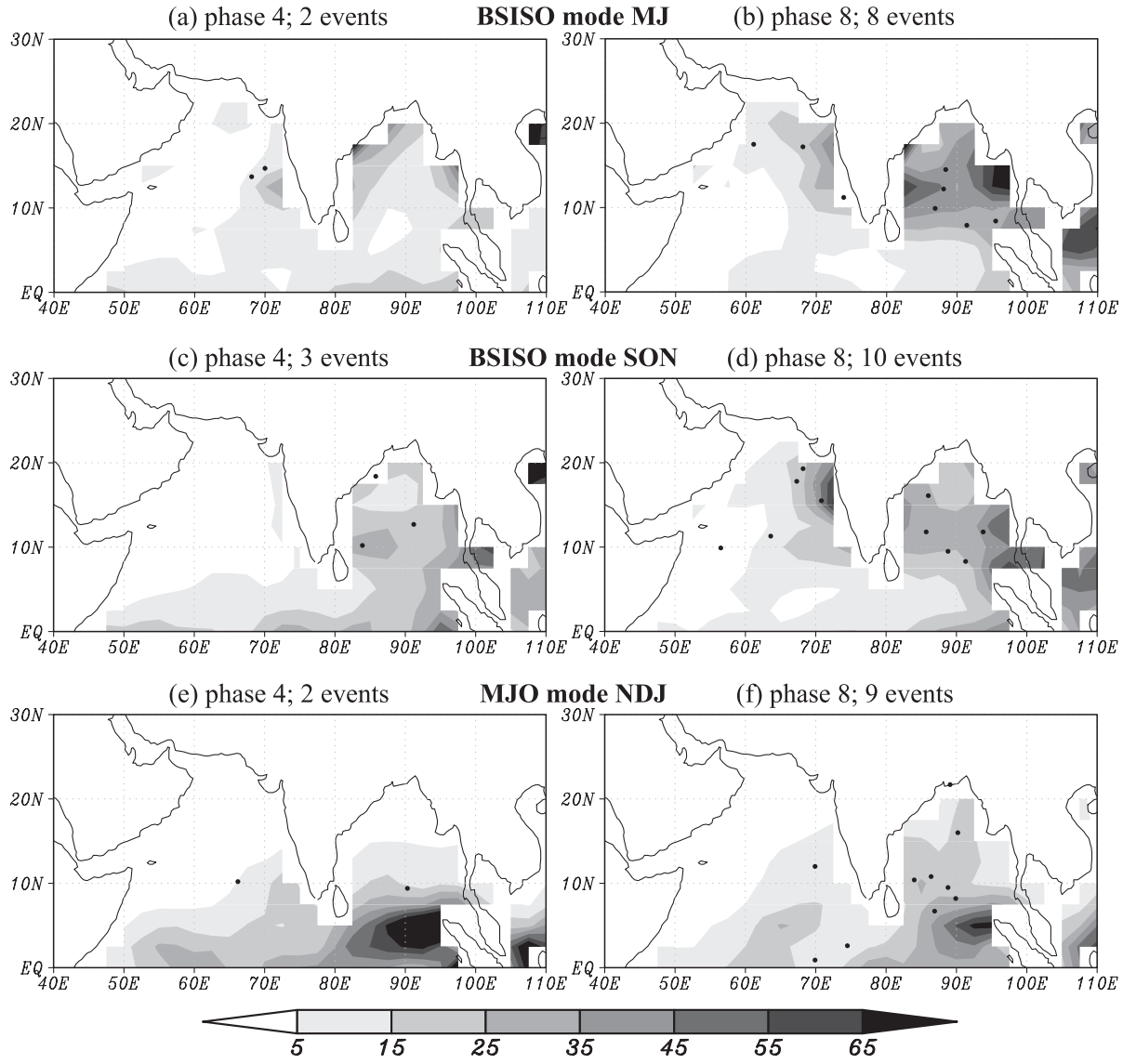

Fig. 10. Horizontal distribution of composite genesis potential index (GPI) with reference to the inactive (active) phase for TC formation in left (right) panels associated with the BSISO mode during May–June (upper panels) and September–November (middle panels) and the MJO mode during November–January (lower panels). A composite was constructed using daily GPI data for the period 1982–2008 in the same way as in Fig. 7. TC formation events that occurred in association with the corresponding mode during the corresponding season for the period 1979–2008 are denoted by solid dots.

reference to the TCs formed in the central Bay of Bengal (major TC formation location) in phase 8 for both BSISO and MJO modes. The treatment made here makes it possible to represent synoptic-scale disturbances, that are cancelled out in a popular composite method like that used in Figs. 7 and 8. Further, note that using NCEP-DOE reanalysis data reproduces consistent results.

In both cases, synoptic-scale cyclonic disturbances can be traced back at least six days prior to TC formation (tropical-depression strength). In the BSISO case, a major convective area is located along the equator on −6 day. A pair of cyclonic circulations appear in both hemispheres and makes a strong westerly wind burst near the equator. The zonally elongated shape of the cyclonic circulation

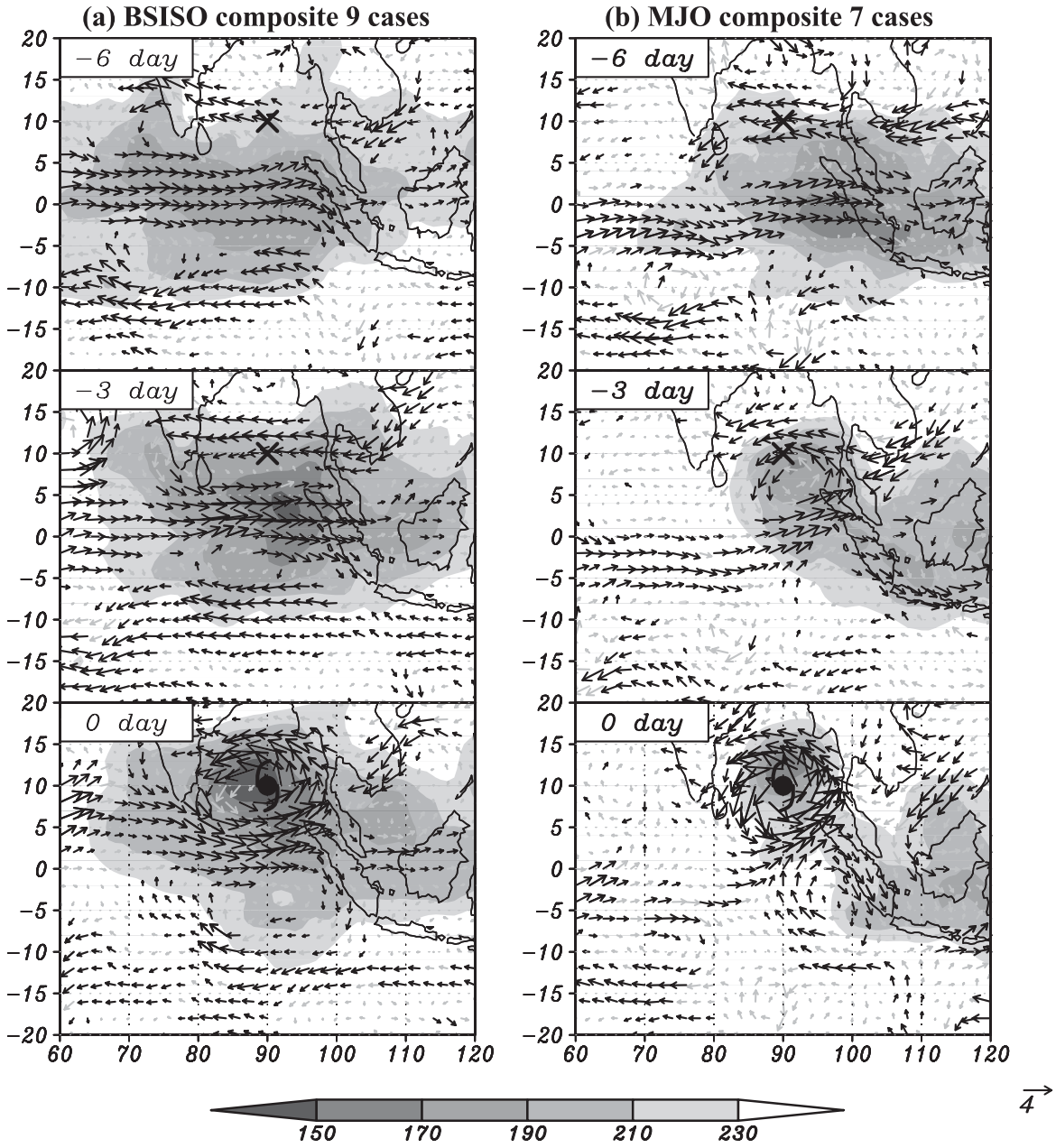

Fig. 11. Horizontal structure of OLR (shading) and 850-hPa wind (vectors) for the composite TC genesis scenario associated with the (a) BSISO and (b) MJO modes. A composite is constructed with reference to the TCs that formed in the central Bay of Bengal (5°–15°N, 80°–100°E) in phase 8. The abscissa and ordinate are relative longitude and latitude, respectively, with reference to the mean TC formation location (10°N, 90°E). Maps are drawn for convenience. The data used for the composite is unfiltered OLR and disturbance component of the horizontal winds based on the separation method developed by Kurihara et al. (1993). Statistically significant winds (either u or v) at 90% confidence level are denoted by thick vectors.

partly reflects the diversity of each sample in the zonal location. Three days later, the convection moves eastward with the strengthened westerly wind burst. On 0 day, the deep convective center coincides with the TC formation location and coincides with the center of the low-level cyclonic

circulation. Therefore, the seed disturbance in the BSISO case is the shear vorticity associated with the enhanced equatorial westerly burst. This is similar to the Nargis-formation scenario (Kikuchi et al. 2009) and confirms that Nargis is a typical case.

In the MJO case, on the other hand, the feature is somewhat different. On −6 day, a convection anomaly is present just to the west of the Maritime Continent. A cyclonic circulation flowing into the convection is seen in the northern hemisphere. On −3 day, a cyclonic circulation together with the associated convection is present near the location of the TC formation. As expected from Fig. 8 and Fig. 2b, the main convective area is present far to the east of the TC-formation location at this time. Thus, this seed cyclonic circulation appears as a residual disturbance of the MJO. Similarly, different sources reports that westward propagating residual disturbances of the TCs that occur in the western North Pacific transformed into monsoon depressions in the Bay of Bengal (Krishnamurti et al. 1977; Saha et al. 1981; Chen and Weng 1999). Note that the off-equatorial residual component shown in Fig. 11b closely resembles the moist Rossby waves that emanate from the equatorial Kelvin-Rossby wave packet (Wang and Li 1994; Wang and Xie 1997). We interpret it as a convectively coupled Rossby wave that escaped from the major convective complex of the MJO, which can only occur when the major body of the MJO passes through the Indian Ocean (in the dry phase 8).

In conclusion, from common features in both modes, the ISO appears to have the potential of provide a synoptic-scale disturbance accompanying an organized convection that acts as a seed for TC genesis. The synoptic disturbance provided by the BSISO mode is a cyclonic vorticity anomaly located to the north of the prominent equatorial westerly wind burst when the Indian Ocean is in a wet phase. The disturbance provided by the MJO mode is a convectively coupled Rossby wave low that escaped from the major body of the MJO mode situated over the Maritime Continent when the Indian Ocean is in a dry phase. Although the composite is based only on the specific phase, it can be easily imagined that the same process takes place for other wet phases of the BSISO mode. Together with the results from the previous subsection, we can conclude that the BSISO mode enhances TC formation by modifying the environmental forcing and providing a seed disturbance. The MJO mode, in contrast, enhances TC formation only by providing a seed disturbance.

6. Summary

To improve our understanding of TC genesis in the northern Indian Ocean (NIO), a statistical analysis based on 30 years (from 1979 to 2008) of data was carried out to elucidate the relationship with the tropical intraseasonal oscillation (ISO). Special attention has also been paid to comparing the result with TC Nargis, which emerged in the Bay of Bengal in April 2008. Because the literature documenting TC behaviors in the NIO are very limited, the genesis potential, maximum potential intensity, and prevailing tracks are also addressed in an attempt to relate them to environmental forcing.

While the number of TC genesis events is primarily concentrated during fall, strong storms tend to occur in spring, especially in April due to favorable large-scale circulation for TC development taking place in the pre-monsoon season. In addition, these TCs tend to hit the west coast of the Indochina Peninsula due to the prevailing steering flow (Yamada et al. 2010). Nargis was one of them and occurred under an abnormally conducive environmental conditions for April. Nargis is considered to be a typical TC in April in terms of intensity and motion.

Another important aspect with reference to Nargis formation revealed using a long-term dataset is the connection with the ISO. In this study, two types of ISO modes were objectively and quantitatively defined: the BSISO mode represents a typical boreal summer ISO, and the MJO mode represents a typical boreal winter ISO. Over 60% of TCs occur in association with the two ISO modes, but the majority of them (over 70%) are attributed to the BSISO mode. The BSISO mode primarily affects TC formation in May–June and September–November, while the MJO mode affects TC formation primarily from November–December. April and November are transitional months in which both the BSISO and MJO modes affect TC formation.

BSISO and MJO modes affect TC formation in different ways. For the BSISO mode, TC formation is enhanced when the wet phases of the BSISO mode overlay the NIO. For the MJO mode, TC formation is enhanced only after the MJO convection passes over the Malay Peninsula and when the Indian Ocean is in a dry phase. This is attributed to the fact that the BSISO and MJO modes have dis-

tinctive life cycles and structures. The BSISO mode has a clear northward propagating convection accompanying a cyclonic circulation, which results in a strong wet phase influencing TC formation in the NIO. In contrast, the MJO mode has a predominant eastward propagating feature, which makes a weak wet phase in the NIO, and consequently, has a weaker modulation effect on TC formation.

Distinctive life cycles also make the BSISO and MJO modes affect TC genesis differently. As a large-scale forcing on an intraseasonal time scale, the BSISO mode makes the environmental forcing more conducive for TC genesis during its wet phase while the MJO mode does not. On the other hand, both the BSISO and MJO modes provide a synoptic-scale seed disturbance at least 6 days prior to TC formation. The synoptic disturbance provided by the BSISO mode is a cyclonic vorticity anomaly to the north of the equatorial convection and westerly wind burst, whereas the disturbance provided by the MJO mode is a convectively coupled Rossby wave that breaks away from the major body of the MJO convection. In conclusion, the BSISO mode enhances TC formation not only by modifying environmental forcing but also by providing a seed disturbance. The MJO mode, in contrast, affects TC formation only by providing a seed disturbance. The results support the idea proposed by Kikuchi et al. (2009) that the ISO has a potential ability to influence TC formation more directly by seeding a pre-TC perturbation other than by changing the environmental conditions to facilitate the development of an incipient disturbance.

While not all events are attributed to the ISO, monitoring of the ISO, especially the BSISO mode, will contribute to a better forecast of TC formation in the NIO. To achieve a more comprehensive understanding of TC formation in this region, the role of quasibiweekly waves and mixed Rossby-gravity waves should be taken into consideration in the future.

Acknowledgements

This research was supported by NSF Grant ATM-0647995 and BW acknowledges the support from NASA grant NNX09AG97G. Additional support was provided by the Japan Agency for Marine-Earth Science and Technology (JAMSTEC), by NASA through grant NNX07AG53G, and by NOAA through grant NA17RJ1230 through their sponsorship of research activities at the International Pacific Research Center. Interpolated OLR data, NCEP_Reanalysis 2 data, and NOAA_OI_SST_V2 data provided by the NOAA/OAR/ESRL PSD, Boulder, Colorado, USA, from their website at http://www.cdc.noaa.gov/ are used in this study. JTWC best track data are obtained from http://metocph.nmci.navy.mil/jtwc.php. JRA-25 and JCDAS are provided from the cooperative research project of the JRA-25 long-term reanalysis by Japan Meteorological Agency (JMA) and Central Research Institute of Electric Power Industry (CRIEPI) and available from their Web site at http://jra.kishou.go.jp/JRA-25/index_en.html. A Fortran code to calculate the MPI is obtained from K. A. Emanuel's ftp site at ftp://texmex.mit.edu/pub/emanuel/. KK acknowledges the support by Dr. Satoh at JAMSTEC who gave him the opportunity to visit JAMSTEC. He was also inspired by discussions with Drs. Taniguchi, Tomita, Nasuno, and Oouchi during his stay. We would also like to thank two anonymous reviewers for giving insightful comments that helped improve this manuscript, and to Ms. May Izumi for her editorial work.

References

Adem, J., 1956: A series solution for the barotropic vorticity equation and its application in the study of atmospheric vortices. *Tellus*, **8**, 364–372.

Avila, L. A., 1991: Eastern North Pacific hurricane season of 1990. *Monthly Weather Review*, **119**, 2034–2046.

Bergeron, T., 1954: The problem of tropical hurricanes. *Quarterly Journal of the Royal Meteorological Society*, **80**, 131–164.

Bessafi, M., and M. C. Wheeler, 2006: Modulation of south Indian ocean tropical cyclones by the Madden-Julian oscillation and convectively coupled equatorial waves. *Mon. Wea. Rev.*, **134**, 638–656.

Bister, M., and K. A. Emanuel, 2002: Low frequency variability of tropical cyclone potential intensity. 1. Interannual to interdecadal variability. *J. Geophys. Res.*, **107**, 4801, doi:10.1029/2001JD000776.

Brand, S., C. A. Buenafe, and H. D. Hamilton, 1981: Comparison of tropical cyclone motion and environmental steering. *Monthly Weather Review*, **109**, 908–909.

Briegel, L. M., and W. M. Frank, 1997: Large-scale influences on tropical cyclogenesis in the western north Pacific. *Mon. Wea. Rev.*, **125**, 1397–1413.

Camargo, S. J., K. A. Emanuel, and A. H. Sobel, 2007a: Use of a genesis potential index to diagnose ENSO effects on tropical cyclone genesis. *J. Climate*, **20**, 4819–4834.

Camargo, S. J., A. H. Sobel, A. G. Barnston, and K. A. Emanuel, 2007b: Tropical cyclone genesis potential index in climate models. *Tellus*, **59**, 428–443.

Camp, J. P., and M. T. Montgomery, 2001: Hurricane maximum intensity: Past and present. *Monthly Weather Review*, **129**, 1704–1717.

Chen, T. C., and S. P. Weng, 1999: Interannual and intraseasonal variations in monsoon depressions and their westward-propagating predecessors. *Monthly Weather Review*, **127**, 1005–1020.

Dengler, K., and M. J. Reeder, 1997: The effects of convection and baroclinicity on the motion of tropical-cyclone-like vortices. *Quarterly Journal of the Royal Meteorological Society*, **123**, 699–725.

Dickinson, M., and J. Molinari, 2002: Mixed Rossby-gravity waves and Western Pacific tropical cyclogenesis. Part I: Synoptic evolution. *J. Atmos. Sci.*, **59**, 2183–2196.

Duchon, C. E., 1979: Lanczos Filtering in One and two Dimensions. *J. Appl. Meteorol.*, **18**, 1016–1022.

Emanuel, K., 2000: A statistical analysis of tropical cyclone intensity. *Monthly Weather Review*, **128**, 1139–1152.

Emanuel, K., 2003: Tropical cyclones. *Annual Review of Earth and Planetary Sciences*, **31**, 75–104.

Emanuel, K. A., 1986: An air sea interaction theory for tropical cyclones. Part I: Steady-state maintenance. *J. Atmos. Sci.*, **43**, 585–604.

Emanuel, K. A., 1997: Some aspects of hurricane inner-core dynamics and energetics. *J. Atmos. Sci.*, **54**, 1014–1026.

Emanuel, K. A., and D. S. Nolan, 2004: Tropical cyclone activity and global climate. *Proc. of 26th Conference on Hurricanes and Tropical Meteorology*, American Meteorological Society, Miami, FL.

Frank, W. M., and P. E. Roundy, 2006: The role of tropical waves in tropical cyclogenesis. *Monthly Weather Review*, **134**, 2397–2417.

Fu, X., and B. Wang, 2004: The boreal-summer intraseasonal oscillations simulated in a hybrid coupled atmosphere-ocean model. *Mon. Wea. Rev.*, **132**, 2628–2649.

George, J. E., and W. M. Gray, 1976: Tropical cyclone motion and surrounding parameter relationships. *Journal of Applied Meteorology*, **15**, 1252–1264.

Goswami, B. N., 2005: South Asian summer monsoon: An overview in *The Global Monsoon System: Research and Forecast*, C.-P. Chang, B. Wang, and N.-C. G. Lau, Eds., WMO/TD, No. 1266, 47–71.

Goswami, B. N., R. N. Keshavamurty, and V. Satyan, 1980: Role of barotropic, baroclinic and combined barotropic-baroclinic instability for the growth of monsoon depressions and mid-tropospheric cyclones. *Earth and Planetary Sciences*, **89**, 79–97.

Goswami, B. N., R. S. Ajayamohan, P. K. Xavier, and D. Sengupta, 2003: Clustering of synoptic activity by Indian summer monsoon intraseasonal oscillations. *Geophys. Res. Lett.*, **30**, 1431, doi:10.1029/2002GL016734.

Gray, W. M., 1968: Global view of the origin of tropical disturbances and storms. *Mon. Wea. Rev.*, **96**, 669–700.

Gray, W. M., 1979: Hurricanes: their formation, structure, and likely role in the tropical circulation in *Meteorology over the Tropical Oceans*, D. B. Shaw, Ed., Royal Meteorological Society, 155–218.

Gutzler, D. S., and R. A. Madden, 1989: Seasonal variations in the spatial structure of intraseasonal tropical wind fluctuations. *Journal of the Atmospheric Sciences*, **46**, 641–660.

Hatsushika, H., J. Tsutsui, M. Fiorino, and K. Onogi, 2006: Impact of wind profile retrievals on the analysis of tropical cyclones in the JRA-25 reanalysis. *Journal of the Meteorological Society of Japan*, **84**, 891–905.

Hendon, H. H., and M. L. Salby, 1994: The life cycle of the Madden-Julian oscillation. *J. Atmos. Sci.*, **51**, 2225–2237.

Holland, G. J., 1983: Tropical cyclone motion: Environmental interaction plus a beta effect. *Journal of the Atmospheric Sciences*, **40**, 328–342.

Holland, G. J., 1997: The maximum potential intensity of tropical cyclones. *J. Atmos. Sci.*, **54**, 2519–2541.

Kanamitsu, M., W. Ebisuzaki, J. Woollen, S. K. Yang, J. J. Hnilo, M. Fiorino, and G. L. Potter, 2002: NCEP-DOE AMIP-II reanalysis (R-2). *Bull. Amer. Meteor. Soc.*, **83**, 1631–1643.

Kemball-Cook, S., and B. Wang, 2001: Equatorial waves and air-sea interaction in the boreal summer intraseasonal oscillation. *J. Climate*, **14**, 2923–2942.

Kikuchi, K., and Y. N. Takayabu, 2003: Equatorial circumnavigation of moisture signal associated with the Madden-Julian Oscillation (MJO) during boreal winter. *J. Meteor. Soc. Japan*, **81**, 851–869.

Kikuchi, K., and B. Wang, 2009: Global perspective of the quasi-biweekly oscillation. *J. Climate*, **22**, 1340–1359.

Kikuchi, K., B. Wang, and H. Fudeyasu, 2009: Genesis of tropical cyclone Nargis revealed by multiple satellite observations. *Geophys. Res. Lett.*, **36**, doi:10.1029/2009GL037296.

Kiladis, G. N., M. Wheeler, P. T. Haertel, K. H. Straub, and P. E. Roundy, 2009: Convectively coupled equatorial waves. *Reviews of Geophysics*, in press.

Krishnamurti, T. N., J. Molinari, H.-L. Pan, and V. Wong, 1977: Downstream amplification and formation of monsoon disturbances. *Monthly Weather Review*, **105**, 1281–1297.

Kunii, M., Y. Shoji, M. Ueno, and K. Saito, 2010: Mesoscale data assimilation of Myanmar cyclone Nargis. *Journal of the Meteorological Society of Japan*, submitted.

Kurihara, Y., M. A. Bender, and R. J. Ross, 1993:

An Initialization scheme of hurricane models by vortex specification. *Mon. Wea. Rev.*, **121**, 2030–2045.

Kuroda, T., K. Saito, and M. Kunii, 2010: Numerical simulations of Myanmar cyclone Nargis and the associated storm surge Part I: Forecast experiment with NHM and simulation of storm surge. *Journal of the Meteorological Society of Japan*, submitted.

Landsea, C. W., G. D. Bell, W. M. Gray, and S. B. Goldenberg, 1998: The extremely active 1995 Atlantic hurricane season: Environmental conditions and verification of seasonal forecasts. *Mon. Wea. Rev.*, **126**, 1174–1193.

Lau, K. M., and P. H. Chan, 1985: Aspects of the 40–50 day oscillation during the northern winter as inferred from outgoing longwave radiation. *Mon. Wea. Rev.*, **113**, 1889–1909.

Lau, K. M., and P. H. Chan, 1986: Aspects of the 40–50 day oscillation during the northern summer as inferred from outgoing longwave radiation. *Mon. Wea. Rev.*, **114**, 1354–1367.

Liebmann, B., and C. A. Smith, 1996: Description of a complete (interpolated) outgoing longwave radiation dataset. *Bull. Amer. Meteor. Soc.*, **77**, 1275–1277.

Lin, II, C. H. Chen, I. F. Pun, W. T. Liu, and C. C. Wu, 2009: Warm ocean anomaly, air sea fluxes, and the rapid intensification of tropical cyclone Nargis (2008). *Geophysical Research Letters*, **36**, L03817, doi:10.1029/2008GL035815.

Locarnini, R. A., A. V. Mishonov, J. I. Antonov, T. P. Boyer, and H. E. Garcia, 2006: *World ocean atlas 2005*, *Volume 1: Temperature*. S. Levitus, Ed. NOAA Atlas NESDIS 61, U.S. Government Printing Office, Washington, D. C., 182 pp.

Madden, R. A., and P. R. Julian, 1971: Detection of a 40–50 day oscillation in the zonal wind in the tropical Pacific. *J. Atmos. Sci.*, **28**, 702–708.

Madden, R. A., and P. R. Julian, 1972: Description of global-scale circulation cells in tropics with a 40–50 day period. *J. Atmos. Sci.*, **29**, 1109–1123.

Mak, M., 1987: Synoptic-scale disturbances in the summer monsoon in *Monsoon Meteorology*, C. P. Chang, and T. N. Krishnamurti, Eds., Oxford Univ. Press, New York, pp. 435–460.

Maloney, E. D., and D. L. Hartmann, 1998: Frictional moisture convergence in a composite life cycle of the Madden-Julian oscillation. *J. Climate*, **11**, 2387–2403.

Maloney, E. D., and D. L. Hartmann, 2000a: Modulation of eastern North Pacific hurricanes by the Madden-Julian oscillation. *J. Climate*, **13**, 1451–1460.

Maloney, E. D., and D. L. Hartmann, 2000b: Modulation of hurricane activity in the Gulf of Mexico by the Madden-Julian oscillation. *Science*, **287**, 2002–2004.

Miller, B. I., 1958: On the maximum intensity of hurricanes. *Journal of Meteorology*, **15**, 184–195.

Molinari, J., and D. Vollaro, 2000: Planetary- and synoptic-scale influences on eastern Pacific tropical cyclogenesis. *Mon. Wea. Rev.*, **128**, 3296–3307.

Molinari, J., D. Knight, M. Dickinson, D. Vollaro, and S. Skubis, 1997: Potential vorticity, easterly waves, and eastern Pacific tropical cyclogenesis. *Mon. Wea. Rev.*, **125**, 2699–2708.

Nolan, D. S., E. D. Rappin, and K. A. Emanuel, 2006: Could hurricanes form from random convection in a warmer world? *Proc. of 27th Conference on Hurricanes and Tropical Meteorology*, 1C.8, American Meteorological Society, Monterey, CA.

Onogi, K., J. Tslttsui, H. Koide, M. Sakamoto, S. Kobayashi, H. Hatsushika, T. Matsumoto, N. Yamazaki, H. Kaalhori, K. Takahashi, S. Kadokura, K. Wada, K. Kato, R. Oyama, T. Ose, N. Mannoji, and R. Taira, 2007: The JRA-25 reanalysis. *Journal of the Meteorological Society of Japan*, **85**, 369–432.

Palm'en, T., 1948: On the formation and structure of tropical hurricanes. *Geophysica*, **3**, 26–39.

Reale, O., W. K. Lau, J. Susskind, E. Brin, E. Liu, L. P. Riishojgaard, M. Fuentes, and R. Rosenberg, 2009: AIRS impact on the analysis and forecast track of tropical cyclone Nargis in a global data assimilation and forecasting system. *Geophysical Research Letters*, **36**, L06812, doi:10.1029/2008GL037122.

Reynolds, R. W., N. A. Rayner, T. M. Smith, D. C. Stokes, and W. Q. Wang, 2002: An improved in situ and satellite SST analysis for climate. *Journal of Climate*, **15**, 1609–1625.

Riehl, H., 1948: On the formation of typhoons. *Journal of Meteorology*, **5**, 247–264.

Ritchie, E. A., and G. J. Holland, 1999: Large-scale patterns associated with tropical cyclogenesis in the western Pacific. *Mon. Wea. Rev.*, **127**, 2027–2043.

Rotunno, R., and K. A. Emanuel, 1987: An air-sea interaction theory for tropical cyclones. Part II. Evolutionary study using a nonhydrostatic axisymmetrical numerical model. *J. Atmos. Sci.*, **44**, 542–561.

Saha, K., F. Sanders, and J. Shukla, 1981: Westward propagating predecessors of monsoon depressions. *Monthly Weather Review*, **109**, 330–343.

Saito, K., T. Kuroda, M. Kunii, and N. Kohno, 2010: Numerical simulation of Myanmar cyclone Nargis and the associated storm surge Part 2: Ensemble prediction. *Journal of the Meteorological Society of Japan*, submitted.

Salby, M. L., and H. H. Hendon, 1994: Intraseasonal behavior of clouds, temperature, and motion in the tropics. *J. Atmos. Sci.*, **51**, 2207–2224.

Shi, W., and M. H. Wang, 2008: Three-dimensional observations from MODIS and CALIPSO for ocean responses to cyclone Nargis in the Gulf of Marta-

ban. *Geophysical Research Letters*, **35**, L21603, doi:10.1029/2008GL035279.

Shukla, J., 1987: Interannual variability of monsoon in *Monsoons*, J. S. Fein and P. L. Stephens, Eds., John Wiley, New York, pp. 399–464.

Sikka, D. R., and S. Gadgil, 1980: On the maximum cloud zone and the ITCZ over Indian longitudes during the southwest monsoon. *Mon. Wea. Rev.*, **108**, 1840–1853.

Takayabu, Y. N., 1994: Large-scale cloud disturbances associated with equatorial waves. Part I: Spectral features of the cloud disturbances. *J. Meteor. Soc. Japan*, **72**, 433–449.

Takayabu, Y. N., and T. Nitta, 1993: 3–5 day-period disturbances coupled with convection over the tropical Pacific Ocean. *J. Meteor. Soc. Japan*, **71**, 221–246.

Taniguchi, H., W. Yanase, and M. Satoh, 2010: Ensemble simulation of cyclone Nargis by a global cloud-system-resolving model—modulation of cyclogenesis by the Madden-Julian oscillation. *Journal of the Meteorological Society of Japan*, submitted.

Thorncroft, C., and K. Hodges, 2001: African easterly wave variability and its relationship to Atlantic tropical cyclone activity. *J. Climate*, **14**, 1166–1179.

Wang, B., and H. Rui, 1990: Synoptic climatology of transient tropical intraseasonal convection anomalies: 1975–1985. *Meteor. Atmos. Phys.*, **44**, 43–61.

Wang, B., and X. F. Li, 1992: The beta drift of three-dimensional vortices: A numerical study. *Monthly Weather Review*, **120**, 579–593.

Wang, B., and T. Li, 1994: Convective interaction with boundary-layer dynamics in the development of a tropical intraseasonal system. *J. Atmos. Sci.*, **51**, 1386–1400.

Wang, B., and X. Xie, 1997: A model for the boreal summer intraseasonal oscillation. *J. Atmos. Sci.*, **54**, 72–86.

Wang, B., T. Li, Y. H. Ding, R. H. Zhang, and H. J. Wang, 2005: East Asian-Western North Pacific monsoon: A distinctive component of the Asian-Australian monsoon system in *The Global Monsoon System: Research and Forecast*, C.-P. Chang, B. Wang, and N.-C. G. Lau, Eds., WMO/TD, No. 1266, 72–94.

Wang, B., P. J. Webster, K. Kikuchi, T. Yasunari, and Y. Qi, 2006: Boreal summer quasi-monthly oscillation in the global tropics. *Climate Dynamics*, in press.

Wang, Y. Q., and G. J. Holland, 1996: Tropical cyclone motion and evolution in vertical shear. *Journal of the Atmospheric Sciences*, **53**, 3313–3332.

Weare, B. C., and J. S. Nasstrom, 1982: Examples of extended empirical orthogonal function analyses. *Monthly Weather Review*, **110**, 481–485.

Webster, P. J., 2008: Myanmar's deadly daffodil. *Geoscience*.

Weickmann, K. M., G. R. Lussky, and J. E. Kutzbach, 1985: Intraseasonal (30–60 Day) Fluctuations of Outgoing Longwave Radiation and 250-Mb Stream-Function During Northern Winter. *Mon. Wea. Rev.*, **113**, 941–961.

Wheeler, M., and G. N. Kiladis, 1999: Convectively coupled equatorial waves: Analysis of clouds and temperature in the wavenumber-frequency domain. *J. Atmos. Sci.*, **56**, 374–399.

Wheeler, M. C., and H. H. Hendon, 2004: An all-season real-time multivariate MJO index: Development of an index for monitoring and prediction. *Mon. Wea. Rev.*, **132**, 1917–1932.

Yamada, H., Q. Moteki, and M. Yoshizaki, 2010: The peculiar track and rapid intensification of Cyclone Nargis (2008) in the Bay of Bengal. *Journal of the Meteorological Society of Japan*, submitted.

Yanase, W., H. Taniguchi, and M. Satoh, 2010: Environmental modulation and numerical predictability associated with the genesis of tropical cyclone Nargis (2008). *Journal of the Meteorological Society of Japan*, submitted.

Yasunari, T., 1979: Cloudiness fluctuations associated with the northern hemisphere summer monsoon. *J. Meteor. Soc. Japan*, **57**, 227–242.

Yokoi, S., and Y. N. Takayabu, 2010: Environmental and external factors in the genesis of tropical cyclone Nargis in April 2008 over the Bay of Bengal. *Journal of the Meteorological Society of Japan*, submitted.

Yoshida, R., Y. Oku, T. Takemi, and H. Ishikawa, 2010: Satellite and modeling analyses of elliptical eye of devastating cyclone Nargis (2008). *Journal of the Meteorological Society of Japan*, submitted.

Zhang, C. D., and M. Dong, 2004: Seasonality in the Madden-Julian oscillation. *J. Climate*, **17**, 3169–3180.

Zhou, X. Q., and B. Wang, 2007: Transition from an eastern Pacific upper-level mixed Rossby-gravity wave to a western Pacific tropical cyclone. *Geophys. Res. Lett.*, **34**, L24801, doi:10.1029/2007GL031831.